Draft version February 5, 2008
Preprint typeset using LaTeX style emulateapj v. 6/22/04

arXiv:astro-ph/0509650v3 11 Nov 2005

IMPRINTS OF ENVIRONMENT ON CLUSTER AND FIELD LATE-TYPE GALAXIES AT $Z \sim 1$

N. L. Homeier[1] M. Postman[2], F. Menanteau[1], J. P. Blakeslee[1] S. Mei[1], R. Demarco[1], H. C. Ford[1], G. D. Illingworth[3], A. Zirm[4]

(Dated: Accepted by the Astronomical Journal)
Draft version February 5, 2008

ABSTRACT

We present a comparison of late-type galaxies (Sa and later) in intermediate redshift clusters and the field using images from the Advanced Camera for Surveys (ACS) aboard the *Hubble Space Telescope* (HST). Cluster and field galaxies are selected by matching photometric and spectroscopic catalogs of four cluster fields: CL0152-1357, CL1056-0337 (MS1054), CL1604+4304, and CL1604+4321. Concentration, asymmetry, and clumpiness parameters are calculated for each galaxy in blue (F606W or F625W) and red (F775W or F814W) filters. Galaxy half-light radii, disk scale lengths, color gradients, and overall color are compared. We find marginally significant differences in the asymmetry distributions of spiral and irregular galaxies in the X-ray luminous and X-ray faint clusters. The massive clusters contain fewer galaxies with large asymmetries. The physical sizes of the cluster and field populations are similar; no significant differences are found in half-light radii or disk scale lengths. The most significant difference is in rest-frame $U-B$ color. Late-type cluster galaxies are significantly redder, ~ 0.3 magnitudes at rest-frame $U-B$, than their field counterparts. Moreover, the intermediate-redshift cluster galaxies tend to have blue inward color gradients, in contrast to the field galaxies, but similar to late-type galaxies in low redshift clusters. These blue inward color gradients are likely to be the result of enhanced nuclear star formation rates relative to the outer disk. Based on the significant rest-frame color difference, we conclude that late-type cluster members at $z \sim 0.9$ are not a pristine infalling field population; some difference in past and/or current star formation history is already present. This points to high redshift "groups", or filaments with densities similar to present-day groups, as the sites where the first major effects of environment are imprinted.

Subject headings: galaxies: clusters: general; galaxies: evolution; galaxies: spiral; galaxies: elliptical and lenticular, cD

1. INTRODUCTION

Understanding the physical processes that shape present day galaxies is one of modern astronomy's fundamental goals. Galaxy morphology is clearly related to environment (Dressler 1980; Postman & Geller 1984; Whitmore & Gilmore 1991). Few gas-rich galaxies and relatedly, few galaxies with spiral morphologies are found in the cores of rich clusters. To what extent the environment drives galaxy evolution (nurture) or is simply a roadmap for the distribution of galaxy halo masses (nature) is being currently refined.

By observing clusters at high redshift we can directly observe dynamically young structures. There is substantial evidence that overall cluster galaxy populations evolve with redshift. Fractionally more blue galaxies are found in clusters at higher redshifts; this trend is the Butcher-Oemler (B-O) effect (Butcher & Oemler 1984). However, cluster cores do not show a star-forming galaxy B-O effect (Nakata et al. 2005), and the B-O effect depends sensitively on cluster radius (Ellingson et al. 2001; Nakata et al. 2005; Wake et al. 2005). This implies that the Butcher-Oemler galaxies are infalling field galaxies, and indeed, some blue cluster galaxies have been identified as such (Tran et al. 2005). We test whether the late-type population in intermediate redshift clusters is an infalling field population by comparing the properties of cluster and field galaxies at $z \sim 0.9$, currently the highest redshift where a substantial number of clusters are known.

At low redshift there is a color-density relation (e.g. Goto et al. 2004) similar to the well-known morphology-density relation (Dressler 1980), and widespread evidence that star formation rates are lower in cluster and group galaxies than in the field (Balogh et al. 1997, 1998; Hashimoto et al. 1998; Couch et al. 2001; Lewis et al. 2002; Martínez et al. 2002). The morphology-density, color-density, and star formation rate (SFR)-density relations may be caused by physical processes such as galaxy-galaxy interactions and tidal stripping (Moore et al. 1998), starvation (Larson et al. 1980; Bekki et al. 2002), and/or ram pressure stripping (Gunn & Gott 1972; Quilis et al. 2000; Schulz & Struck 2001). Alternatively, morphology, color, and SFR could be determined by the galaxy's halo mass, and this correlates strongly with galaxy density. Fortunately, large surveys have been able to address this issue. Environment is important in determining the evolution of all but the most massive galaxies (with $M > 3 \times 10^{10}$ $M_\odot$) (Kauffmann et al. 2004; Tanaka et al. 2004), but we have yet to determine the physical mechanisms which are responsible for these observed environmental effects.

The study of galaxy properties and environment from the SDSS by Kauffmann et al. (2004) has shown that the

---

[1] Department of Physics and Astronomy, Johns Hopkins University, 3400 North Charles Street, Baltimore, MD 21218.
[2] STScI, 3700 San Martin Drive, Baltimore, MD 21218.
[3] UCO/Lick Observatory, University of California, Santa Cruz, CA 95064.
[4] Leiden Observatory, Postbus 9513, 2300 RA Leiden, Netherlands.

galaxy property that is most sensitive to environment is star formation history. Star formation in galaxies less massive than 3×10^10 M$_\odot$ and in regions of enhanced local (< 1 Mpc) galaxy density appears to decline gradually over a long, 1-3 Gyr, timescale. This is indicated by the lack of variation in the relationships between indicators of current and recent star formation in all environments. This has important implications for the dominant transformation process(es). Ram pressure stripping is thought to operate on short, < 1 Gyr timescales, while other mechanisms, such as starvation or galaxy harassment, are thought to shut off star formation on longer timescales. However, as a caveat, recent simulations show that a truncated gas disk can persist for a few Gyr (Roediger & Hensler 2005).

Another way to determine which physical processes drive galaxy evolution is to identify the physical characteristics of the regions in which galaxy properties change. Several groups have reported a "break" in the otherwise smooth distribution of the fraction of galaxies with Hα emission with local galaxy density (Gómez et al. 2003; Balogh et al. 2004; Tanaka et al. 2004), with fewer Hα-emitters in higher density regions. However, among the population with significant star formation, no correlation between Hα equivalent width and density was found. The interpretation is that the timescale for the transition from star-forming to non-star-forming is rapid, < 1 Gyr. This is in conflict with the results of Kauffmann et al. (2004) that star formation is gradually extinguished.

Extending these studies to higher redshifts allows us to observe how these trends evolve and trace how they are established. We now know that the morphology-density relation exists at intermediate redshifts (Dressler et al. 1997; Smith et al. 2005; Postman et al. 2005), and evolves smoothly with redshift (Smith et al. 2005; Postman et al. 2005). However, the elliptical fraction as a function of density does not evolve significantly (Postman et al. 2005), and the change in the morphology-density relation between $z \sim 1$ and the present-day universe is in the relative fractions of S0 and spiral+irregular galaxies. The trend of reduced SFR for galaxies in clusters is also established at these redshifts (Ellingson et al. 2001; Postman et al. 2001), although the evolution of total cluster SFRs with redshift is not yet clear (Finn, Zaritsky, & McCarthy 2004; Kodama et al. 2004; Homeier et al. 2005; Finn et al. 2005).

Detailed morphological measurements of cluster galaxies at $z \sim 1$ have recently become possible with the installation of the Advanced Camera for Surveys (ACS; Ford et al. 2003) on the HST. The ACS intermediate redshift cluster survey probes 7 clusters in the redshift range $0.83 \leq z \leq 1.27$. Previous papers in this series have discussed the evolution of the cluster color-magnitude relation at $z = 1.24$ (Blakeslee et al. 2003b), the fundamental plane (Holden et al. 2005), the size-surface brightness relation for early-type cluster galaxies (Holden et al. 2005), the star-forming cluster galaxy population (Homeier et al. 2005), the cluster galaxy luminosity function (Goto et al. 2005), and the morphology-density relation (Postman et al. 2005). In this paper we explore morphological similarities and differences between spiral and irregular galaxies at intermediate redshifts in galaxy clusters and in the field. We compare quantitative morphological measurements, physical sizes, and colors of late-type galaxies in two X-ray luminous clusters at $z = 0.84$, two X-ray faint clusters at $z = 0.9$, and field galaxies at comparable redshifts. We aim to uncover whether these late-type cluster members have properties that make them distinct from late-type field galaxies, or if they are indistinguishable, in which case they are consistent with a pristine infalling field population. If they are already distinct from the field population, it supports the scenario where environmental changes impact galaxies on long, > 1 Gyr timescales.

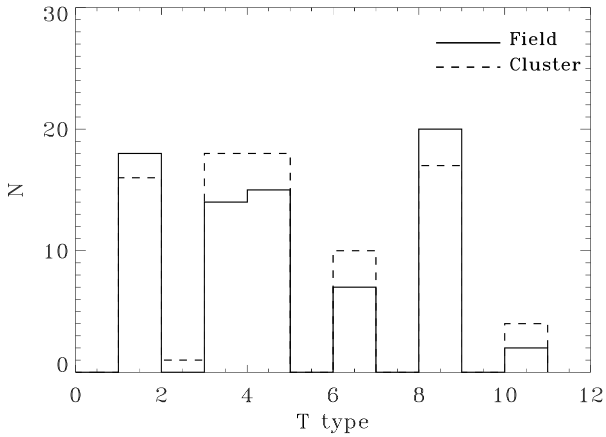

Fig. 1.— The visually classified T-type distributions for the combined cluster (dashed) and field (solid) samples. There is no significant difference in the T-type distributions. The median T-type for the cluster sample is 4, and also for the field sample, 4. This illustrates that there is no significant difference in visual morphology between the field and cluster samples.

2. OBSERVATIONS AND REDUCTIONS

CL0152-1357 (CL0152), CL1056-0337 (MS1054), CL1604+4304, and CL1604+4321 were observed with the ACS Wide Field Channel as part of a guaranteed time observation program (proposal 9290). CL1604+4304 and CL1604+4321 were observed with a single pointing in the V_{606} and I_{814} filters for two orbits each. For CL0152-1357 and MS1054, the observations were taken in a 2×2 (four pointing) mosaic pattern, with 2 orbits of integration in the r_{625} (CL0152), 1 orbit of V_{606} (MS1054), and 2 orbits each of i_{775} and z_{850} filters. The cluster cores were imaged for a total of 32 orbits in each filter because of the $1'$ of overlap between the pointings. The data were processed with the *Apsis* pipeline (Blakeslee et al. 2003a). Our photometry is calibrated to the AB magnitude system using zeropoints in Sirianni et al. (2005). Object detection and photometry was performed by SExtractor (Bertin & Arnouts 1996) incorporated within the *Apsis* pipeline. A more detailed description can be found in Benítez et al. (2004). We use isophotal magnitudes, MAG_ISO, when quoting colors as they provide a more accurate measure of galaxy color, and MAG_AUTO when quoting broad-band magnitudes, as this is the best estimate of a galaxy's total magnitude (Benítez et al. 2004).

2.1. *Sample Selection*

We list the properties of our sample galaxies in Tables 2-9, and show color cutouts in Figures **??**-**??**. **Fig-**

ures 10-17 will appear in the online manuscript, and are not in the astro-ph version. Spectroscopic redshift catalogs were used to select cluster and field samples for CL0152-1357 (Demarco et al. 2005), MS1054 (Tran et al. 1999), CL1604+4304 and CL1604+4321 (Postman et al. 1998; Lubin et al. 1998; Postman et al. 2001). Extensive visual morphology catalogs were created by MP (Postman et al. 2005). Morphologies were determined visually on the T-type system (de Vaucouleurs et al. 1991). All galaxies in the field with i_{775} or $I_{814} \leq 24$ magnitude were classified. Approximately 10% of the galaxies were also classified by three independent classifiers to estimate the classification errors. Majority agreement was achieved for 75% of objects with $i_{775} \leq 23.5$. There was no significant offset between the mean classification from the independent classifiers. More information can be found in Postman et al. (2005).

A T-type $-5 \leq T \leq -3$ corresponds to elliptical galaxies, $-2 \leq \mathrm{T} \leq 0$ corresponds to lenticular (S0) galaxies, and $\mathrm{T} \geq 1$ to Sa and later-type galaxies. We selected field galaxies with visual morphological type Sa or later, T-type ≥ 1, and with redshifts between $0.55 \leq z \leq 1.1$, and excluding the cluster redshift. Histograms of the T-type distributions of cluster and field galaxies are shown in Figure 1. There are no significant differences in the distribution of visually assigned T-types between any of the four cluster galaxy samples and their respective field samples. The median T-type of each sample is $3-4$, except for the CL1604+4304 cluster and field samples, which have medians of 6. The median T-type for the combined cluster sample is 4, and for the combined field sample, also 4.

The field galaxy redshifts were obtained with the same masks as the cluster galaxy redshifts. The advantage of using a field galaxy sample which is taken from the same images as the cluster galaxies is that it minimizes the chance of systematic errors in population properties. The redshift completeness functions for MS1054, CL1604+4304, and CL1604+4321 depend only on R magnitude. There is a color term in the redshift completeness function for CL0152-1357. The mask selection was based on photometric redshift, and galaxies bluer than the red cluster sequence are less likely to have been observed (Demarco et al. 2005; Homeier et al. 2005). About 1/3 of the spectroscopically confirmed late-type population is within 3σ of the red cluster sequence Homeier et al. (2005). Also, in the CL0152-1357 redshift catalog, there is a galaxy group at $z \sim 0.64$ (Demarco et al. 2005). We excluded 9 galaxies with redshifts $0.62 < z < 0.65$ which were likely to be associated with this group. Our final combined field sample contains 71 galaxies.

2.2. *CAS Parameters*

We measured the Concentration (C), Asymmetry (A), and Clumpiness (S) parameters (Abraham et al. 1994; Bershady et al. 2000; Conselice 2003) for all cluster and field galaxies in our sample. Concentration is related to galaxy mass, asymmetry is related to interactions and mergers, and clumpiness is related to the current star formation rate (Conselice 2003). The degree of concentration, asymmetry, or clumpiness increases as the value of the corresponding parameter increases. A public version of the CAS code is available at http://acs.pha.jhu.edu∼felipe/PYCA and described further in (Menanteau et al. 2005).

2.2.1. *C - Concentration*

The concentration definition we use is from Abraham et al. (1994). Concentration is defined as the sum of the galaxy flux within $r_{0.3} = 0.3 \times r_{total}$ divided by the total flux. We fit an ellipse to the Sextractor segmentation map; this is the aperture used for the total flux. The segmentation map includes all pixels assigned to the galaxy that are 1.5σ above the background. The inner radius, $r_{0.3}$, is this aperture with the semi-major and semi-minor axes multipled by 0.3.

2.2.2. *A - Asymmetry*

Qualitatively, one calculates asymmetry by subtracting an 180-degree rotated image from the original image, summing the residuals, and including a correction for the background. We smooth each galaxy image with a gaussian kernel with a width of 1 pixel. This smoothed image is rotated by 180 degrees and subtracted from the smoothed, non-rotated image. The asymmetry forumla we use is, $A = \frac{1}{2}\frac{\Sigma(|I-I_{rot}|)-B_{corr}}{I_t}$, where I is the smoothed image, I_{rot} is this image rotated by 180 degrees, and B_{corr} is a correction factor for the asymmetry signal of the background. $B_{corr} = \sqrt{2} \times Area \times SKYRMS$, and I_t is the sum of the flux in the smoothed image. The asymmetry calculation uses only the pixels included in the Sextractor segmentation map.

2.2.3. *S - Clumpiness*

The clumpiness parameter is a measure of the high frequency residuals in a galaxy image. In our clumpiness calculation we subtract the Sextractor-created background image from the galaxy image. This background-subtracted image is smoothed with a gaussian kernel with FWHM equal to 5% of the total radius (square root of the product of the semi-major and semi-minor axes of the Sextractor Kron aperture). The sum of the pixel values of this background-subtracted, smoothed image is divided by the sum of the pixel values unsmoothed background-subtracted image. Only pixels in the Sextractor segmentation map are used. A formula for the clumpiness parameter can be expressed as, S= $10 \times (\frac{\Sigma(I-I_{back})_{smooth}}{\Sigma(I-I_{back})} \times mask)$, where the mask assures that negative pixels are set to zero before summing and that the central 3×3 pixels are excluded. The central region must be excluded to avoid obtaining anomalously high clumpiness values for galaxies which simply have larger central light concentrations (bulges). What we are interested in is the high frequency light variations from the outer regions of the galaxy, which are related to current star formation rate. We chose 3×3 pixels because it excludes the most problematic region for the majority of our galaxies. This value is then multiplied by 10.

3. RESULTS

3.1. *Colors*

Rest-frame color is a basic parameter of a galaxy and it reflects the integrated star formation history. To

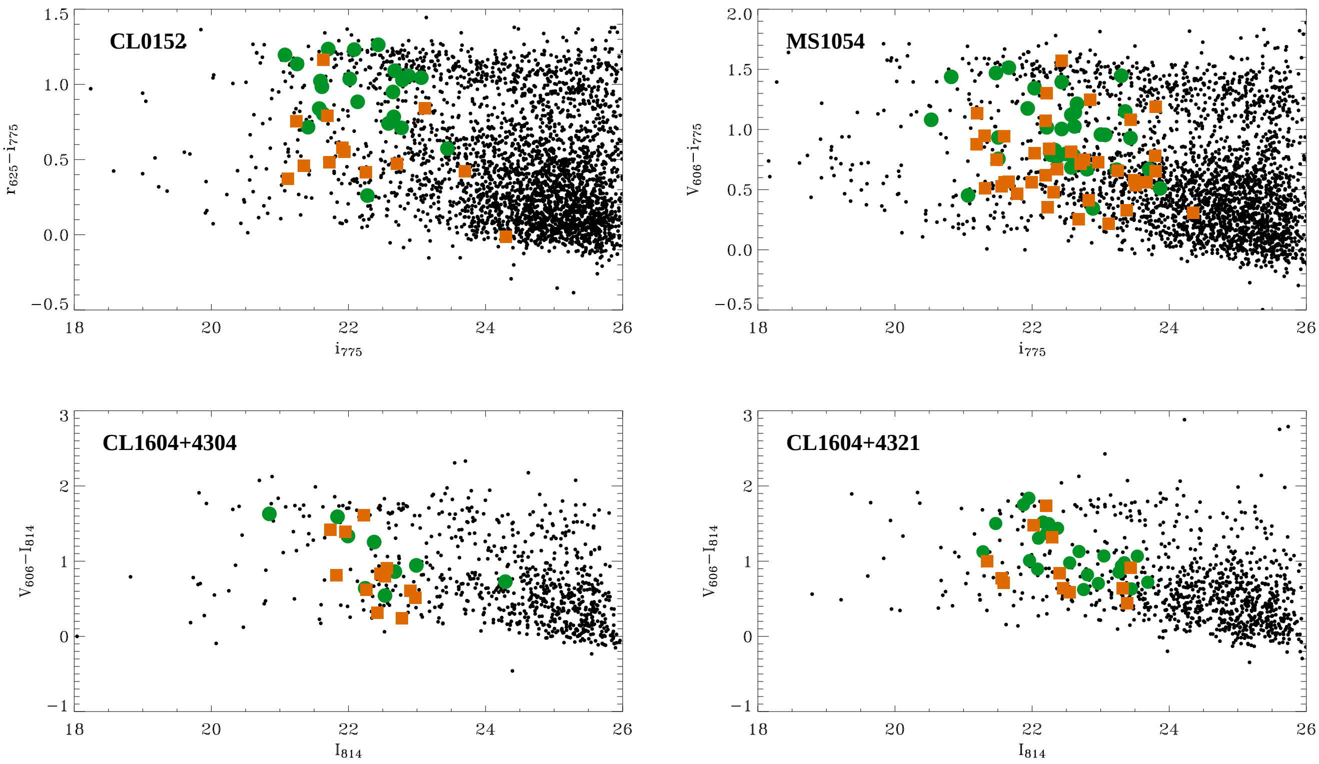

FIG. 2.— Color magnitude diagrams for the cluster fields with the spectroscopically confirmed late-type cluster members as filled dots and the late-type field galaxies as filled squares. This illustrates the colors of the sample galaxies relative to all objects in the field. Note that some of the late-type galaxies are in the red cluster sequence.

compare the colors of the cluster and field galaxies we convert observed magnitudes to rest-frame magnitudes and then colors. We transformed the observed ACS $r_{625}-i_{775}$ (CL0152), $V_{606}-i_{775}$ (MS1054) and $V_{606}-I_{814}$ (CL1604+4304,+4321) to rest-frame $U-B$ (AB magnitudes) colors as follows. Using the IRAF task CALCPHOT, we redshifted the Kinney-Calzetti templates (S0, Sa, Sb, Starb1, and Starb2; Kinney et al. 1996) to the redshift of the galaxy and calculated the observed ACS magnitude using the appropriate filter transmission curves. Also using CALPHOT, we calculated U and B at $z=0$. We then performed a linear fit of the observed ACS color (x-axis) with the rest-frame U or B magnitude minus the observed ACS magnitude (y-axis). In other words, because the observed ACS filters are close to rest-frame U and B filters, we can robustly calculate the difference between the observed ACS magnitude and the rest-frame U or B magnitude. These “corrections” depend somewhat on the spectral slope, which is probed by the observed color. The “corrections” are of the order of 0.5 magnitudes for both filters. In Figure 3 we show the observed colors and redshifts of our sample galaxies and how the observed colors for the Sb (dashed line) and Starb1 (solid line) templates vary with redshift. This illustrates that the chosen templates reasonably cover the range of expected spectral slopes of our sample galaxies.

The terms in the linear transformation equations are listed in Table 1. The transformations are of the form

$$U = m \times c + b + mag_{blue} \qquad (1)$$

TABLE 1
COLOR TRANSFORMATIONS

Cluster	Restframe Band	m	b
CL0152	U	−0.14	0.56
CL0152	B	−0.20	0.61
MS1054	U	−0.30	0.55
MS1054	B	−0.17	0.61
CL1604+4304,21	U	−0.26	0.61
CL1604+4304,21	B	−0.16	0.75

$$B = m \times c + b + mag_{red} \qquad (2)$$

where c is the observed color and mag$_{blue}$ and mag$_{red}$ are the observed magnitudes. For the cluster galaxies we used two transformation equations (for U and B) at redshifts 0.84 (CL0152 and MS1054) and 0.9 (CL1604+4304, +4321). Colors are calculated using the Sextractor isophotal magnitudes, but mag$_{blue}$ and mag$_{red}$ are Sextractor MAG_AUTO magnitudes.

In Figure 4 we show a $(U-B)_z$ histogram, a rest-frame color-magnitude diagram, and a B_z histogram for cluster (dashed line, open dots) and field (solid line, filled dots) galaxies. The field late-type sample is significantly bluer than the cluster late-type sample. Although they also have a slightly different distribution of absolute B magnitude, at a given absolute magnitude the cluster

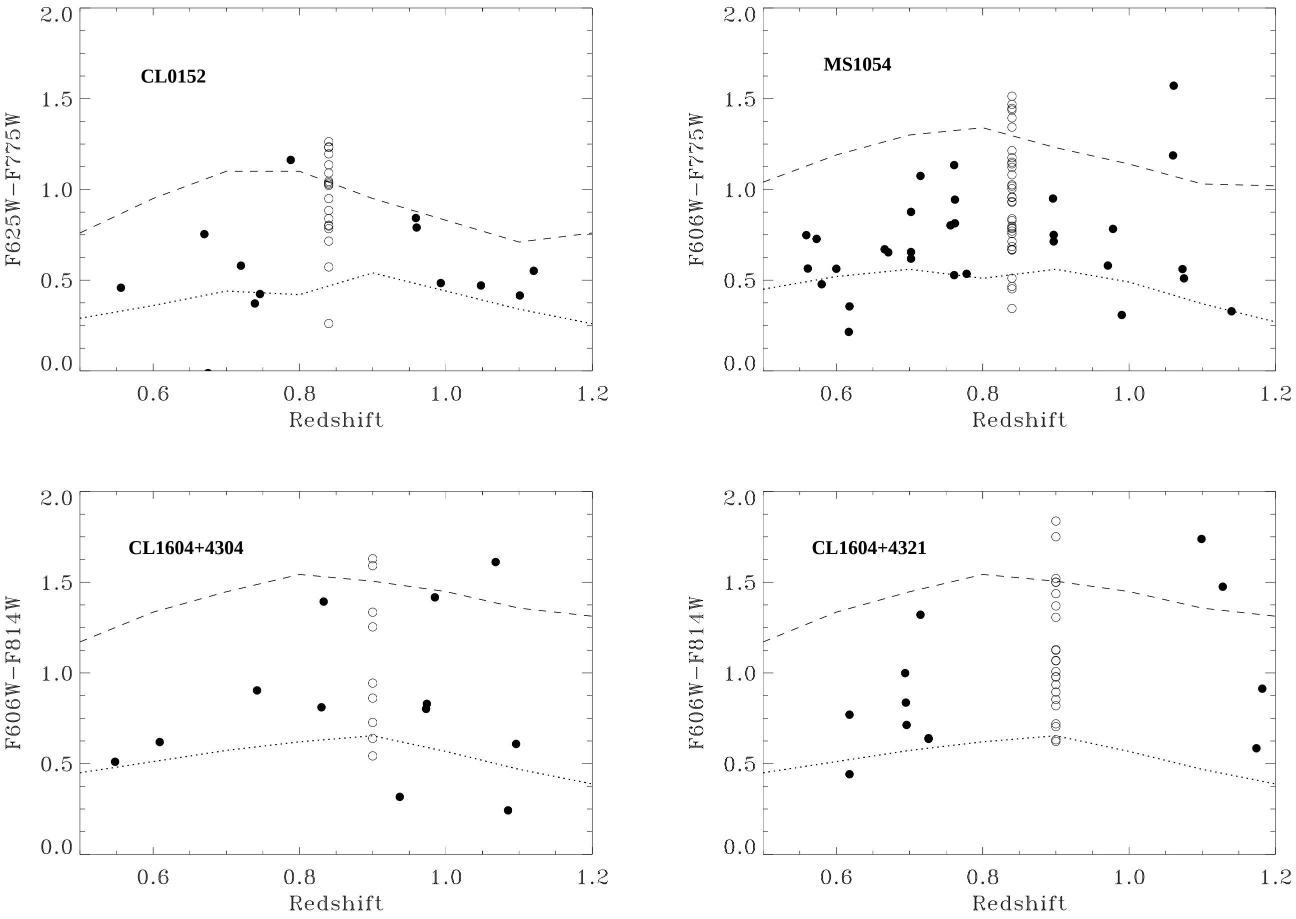

Fig. 3.— Observed ACS color versus redshift for the field (solid dots) and cluster (open dots) galaxies in our sample. Overplotted are the Kinney-Calzetti Sb (dotted) and Starb1 (dashed) templates.

galaxies are redder, as can be seen in the middle panel of Figure 4. There is no significant difference in color distribution between the late-type galaxies in the X-ray luminous and X-ray faint clusters.

The mean rest-frame $U - B$ colors of the cluster and field samples are 0.83 and 0.59 magnitudes, respectively. This difference is highly significant, the K-S test definitely ruling out the null hypothesis that the two samples are drawn from the same parent population, even if we restrict the samples to galaxies with $B_z \leq -20$ (confidence level greater than 99.99%).

However, as mentioned in § 2.1, the redshift completeness for the CL0152 cluster sample is not uniform with magnitude; redder galaxies were more likely to have been observed. This should affect both the cluster and field sample in the CL0152 field, but if we are conservative and exclude the CL0152 cluster galaxies from the combined cluster sample, we still find a highly significant difference between the cluster and field samples. In this case, the mean rest-frame $U - B$ color of the cluster sample is 0.77 magnitudes, compared to 0.59 magnitudes for the field. This gives confidence limit of 99.98%. Including the magnitude cut of $B_z \leq -20$, we have a confidence limit of 99.7%.

This difference persists when the late-type galaxies in the red cluster sequence are excluded. If we include only those galaxies with $(U - B)_z \leq 1$, which removes the red cluster sequence members, this color difference is still highly significant (99.8%). In this case the mean rest-frame $U - B$ colors are 0.68 and 0.53 magnitudes for the cluster and field samples, respectively. Our robust result is that there is a significant offset in rest-frame $U - B$ color between the cluster and field late-type galaxies, in the sense that the cluster galaxies are redder. We found no correlation between rest-frame $U - B$ color and cluster radius or local galaxy density.

3.2. *Cluster-Field CAS Comparison*

Depending on the physical processes affecting cluster galaxies, we might expect offsets from field galaxies in one or more of the CAS parameters. For example, in the low-redshift universe, there is evidence that spiral galaxies in clusters are smoother than their field counterparts (Goto et al. 2003; McIntosh et al. 2004) (S ↓), but some galaxies also have enhanced central star formation (Moss & Whittle 2000; McIntosh et al. 2004; Koopmann & Kenney 2004), which may lead to greater concentration (C ↑). If galaxy-galaxy interactions are important in clusters, cluster galaxies will have greater

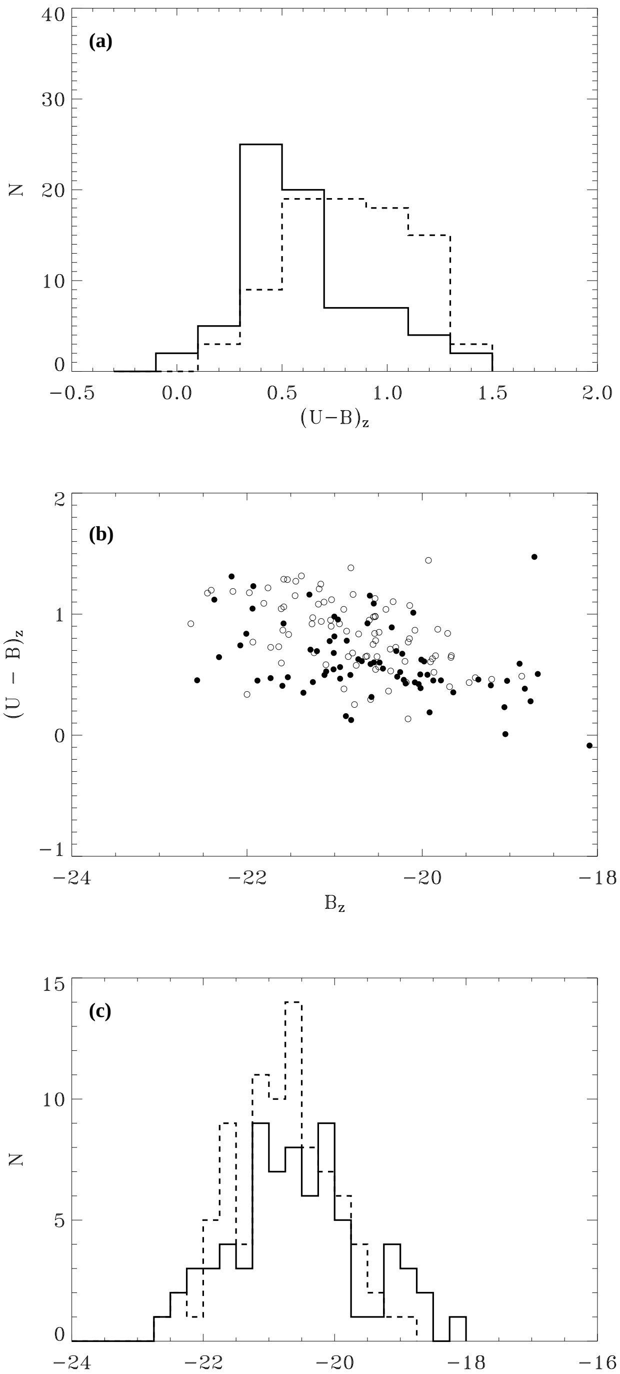

FIG. 4.— Rest-frame U-B vs. B color-magnitude diagram of field (solid line, filled dots) and cluster (dashed line, open dots) galaxies. There is a significant difference in rest-frame $U - B$ color between the cluster and field samples. Although there is also a difference in the range of absolute B magnitude (panel (c)), in panel (b) we can see that at a given B magnitude the cluster galaxies are significantly redder. See text for a discussion of the high significance of this color difference.

asymmetries (A ↑).

In Figure 5 we show histograms of the CAS parameters for galaxies in the field (solid lines), the X-ray faint clusters (CL1604+4304 and CL1604+4321, dashed lines), and the X-ray luminous clusters (CL0152 and MS1054; dotted lines). The distributions of C and S are indistinguishable between any of the groupings (cluster/field, X-ray faint/luminous, X-ray faint/field, X-ray luminous/field) in the blue and red filters (rest-frame U and B). In both blue and red filters there are marginally significant differences between the asymmetry distributions of the combined cluster and field samples, and between the X-ray luminous and X-ray faint clusters.

In the blue filter, the late-type galaxies in the field are more asymmetric than the late-type galaxies in the X-ray luminous clusters (98%), and the late-type galaxies in the X-ray faint clusters are more asymmetric than those in the X-ray luminous clusters (99%). These trends are also marginally significant in the red filter: X-ray luminous vs. field (99.2%), X-ray luminous vs. X-ray faint (92%). There is no significant difference in the asymmetry distributions of the field and the X-ray faint clusters.

We tested whether the difference in asymmetry between the two cluster samples could be due to the difference in filters; F606W is used for CL1604+4304,+4321, and MS1054, while F625W is used for CL0152. A comparison of MS1054 and CL0152, both at $z = 0.84$, with a K-S test shows that we cannot rule out that they are drawn from the same parent population. Therefore, the asymmetry difference cannot be attributed to a difference in filter characteristics.

To recap, the late-type galaxies in the X-ray faint clusters tend to be more asymmetric than their counterparts in the X-ray luminous clusters. If these trends are confirmed after the cluster and field sample sizes are increased, then one possibility for the higher asymmetry values is a greater importance of galaxy-galaxy interactions in these low-mass clusters and in lower density environments, presumably due to the lower relative velocities. The X-ray luminous clusters also have asymmetry distributions that are significantly different than the field, however, in the next section we show that this is related to the color difference between the two samples.

3.2.1. *Asymmetry and Rest-frame Color*

We find a significant difference in asymmetry between the field and X-ray luminous cluster galaxy samples. However, in § 3.1 we showed that there is a significant rest-frame color difference between the cluster and field samples, and in this section we show that this is related to the offset in asymmetry between the X-ray luminous clusters and the field. In Figure 6 we show rest-frame $U - B$ color vs. asymmetry measured in the blue filter for the field (solid dots) and cluster (open dots) galaxies. These two parameters are not independent for the cluster sample. The reddest cluster members have low asymmetries, as might be expected. If we now compare only galaxies bluer than $U - B = 1$, the asymmetry distributions of the field and X-ray luminous cluster samples are indistinguishable. But the asymmetry distributions of the X-ray faint and X-ray luminous clusters are still significantly different (98.7%).

3.2.2. *Asymmetry and Local Galaxy Density*

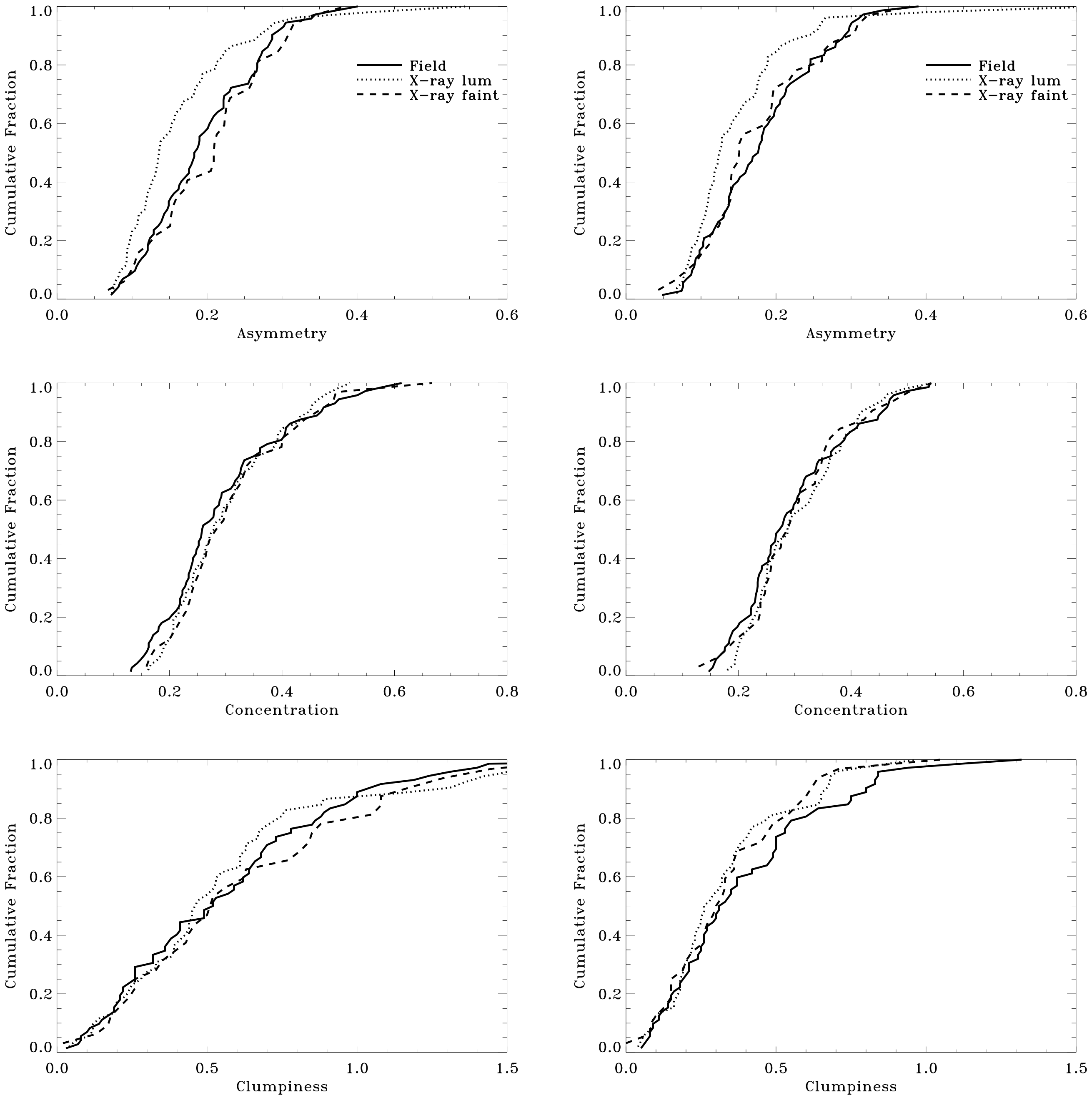

FIG. 5.— Comparison of the individual CAS parameters in the blue (left) and red (right) filters for field (solid line), CL1604+4304 and CL1604+4321 (dashed line), and CL0152-1357 and MS1054 (dotted line). There are marginally significant $(2-2.5\sigma)$ differences in the asymmetry distributions of the combined CL0152,MS1054 and CL1604+4304,+4321 samples (respectively, the X-ray luminous and X-ray faint clusters). There are also significant differences in the asymmetry distributions of the X-ray luminous cluster galaxies and the field galaxies, which is related to the rest-frame color difference. See text for a discussion.

Here we attempt to determine if the asymmetry difference between the two cluster samples could be due to variations in local galaxy density, as measured by Postman et al. (2005). In Figure 7 we plot rest-frame U asymmetry versus local galaxy density for the X-ray faint (stars) and X-ray luminous (filled circles) clusters. The local galaxy densities were measured using a statistical background subtraction, which is described in Postman et al. (2005). There is no statistically significant difference between the local galaxy densities of the two samples.

3.3. *Physical Sizes*

In this section we compare the sizes of cluster and field late-type galaxies. We might expect that disk galaxies in clusters will be smaller due to stripping of stars from galaxy harassment or galaxy-galaxy interactions, a direct effect, or indirectly from the stripping of disk gas,

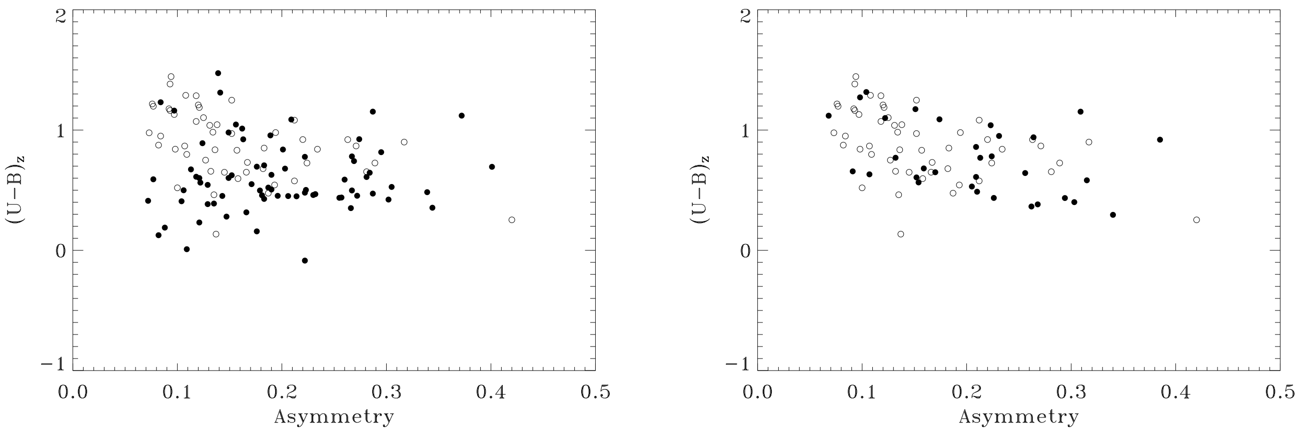

FIG. 6.— Left panel: Comparison of the field (solid dots) and the X-ray luminous cluster galaxies (open dots) asymmetry and rest-frame $U-B$ color. Right panel: Comparison of the X-ray faint (solid dots) and X-ray luminous cluster galaxies (open dots). When galaxies bluer than $U-B=1$ are compared, no significant difference in asymmetry between the two samples is found.

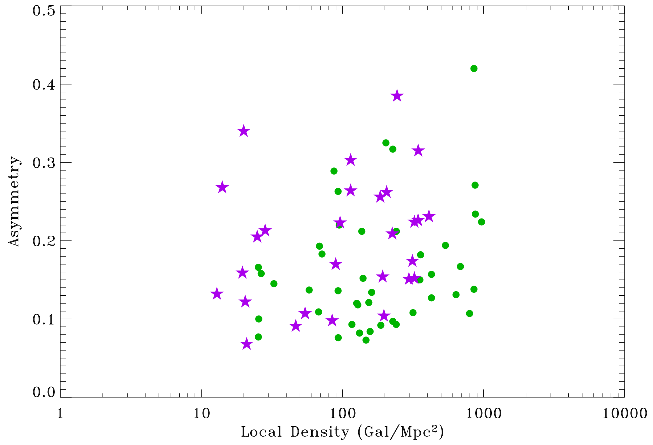

FIG. 7.— Asymmetry values vs. local galaxy density in units of galaxies per Mpc^{-2}. Dots are CL0152 and MS1054 cluster galaxies, and stars are CL1604+4304 and +4321 cluster galaxies. Local galaxy density measurements are from Postman et al. (2005). The densities are calculated with a statistical background subtraction.

preventing future star formation. Indeed, there is some observational evidence that galaxies in the Coma cluster have smaller disks than field galaxies (Gutiérrez et al. 2004).

We compared galaxy sizes in two ways. First, we compared half-light radii from Sextractor, defined as the radius of a circular aperture which encloses 50% of the light. The mean and median half-light radii for all samples in *both* blue and red filters is approximately 3 kpc (no correction for the PSF was made), with no significant differences between the samples.

We also fit PSF-convolved 2D bulge+disk models to the spiral (but not irregular) galaxies using the GALFIT routine (Peng et al. 2002). However, as one can see from the color cutouts in the Appendix, even the spiral galaxies have significant substructure. Many galaxies were not successfully fit with disk or bulge+disk profiles due to bright HII regions and asymmetric structure. This is because we are observing in the rest-frame U and B, where star formation is most apparent. For the galaxies which were successfully fit with disk or bulge+disk models, we compare the disk scale lengths in Figure 8.

In the blue filter, the results of K-S test comparison are that all samples are consistent with being drawn from the same parent population. In the red filter, a K-S test indicates that the probability that the X-ray faint and field disk scale lengths are not drawn from the same parent population is 92%. We do not consider this to be significant, and thus conclude that we find no evidence for any significant differences in disk sizes between the clusters and the field, in either the rest-frame U or B. In summary, the sizes of field and cluster galaxies as measured by half-light radii or disk scale length are indistinguishable.

3.4. *Color Gradients*

There is evidence at $z < 0.1$ that the color gradients of star-forming cluster and field galaxies differ, with field galaxies having red inward color gradients and cluster galaxies having blue inward color gradients (McIntosh et al. 2004). This suggests that the cluster galaxies have larger nuclear star formation rates relative to their outer disks, and is of interest in the discussion of the dominant environmental processes that affect gas-rich cluster galaxies, as well as the growth of bulges and central black holes. Here we test whether the late-type cluster population at $z \sim 0.9$ shows evidence for possessing the same pattern of relatively enhanced nuclear star formation rate by examining their color gradients. The difference in half-light radii at blue and red wavelengths gives a rough measure of the color gradient. We define the color gradient estimate (CGE), CGE= $10\times\log[\frac{r_{eff}^{red}}{r_{eff}^{blue}}]$ similar to McIntosh et al. (2004).

In the left panel of Figure 9 we show the CGE distributions for the cluster (dashed line) and field galaxies (solid line). Interestingly, the field galaxies tend to have

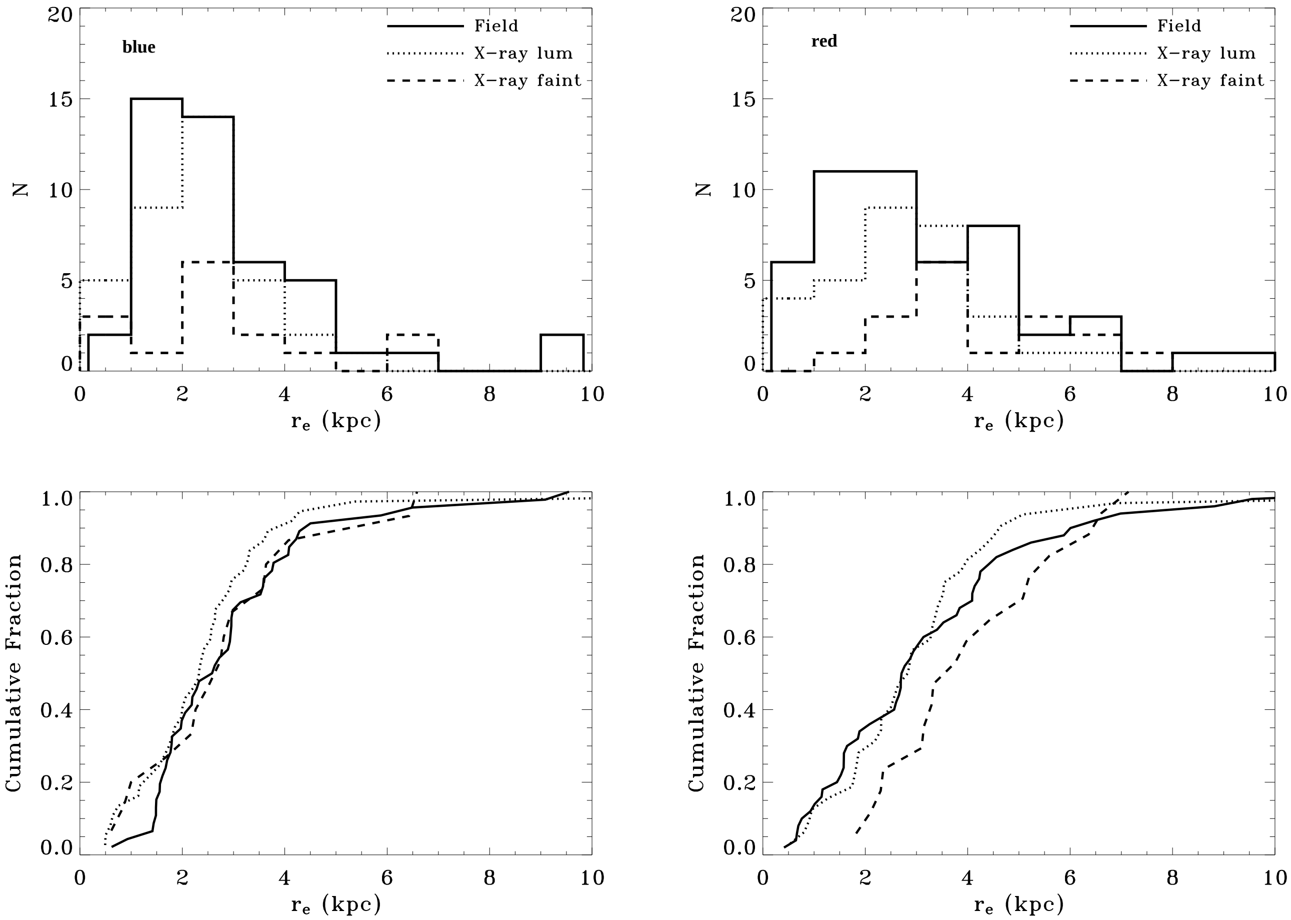

FIG. 8.— Comparison of disk scale lengths in the blue (left panel) and red (right panel) filters for spiral galaxies in the field (solid line), CL1604+4304 and CL1604+4321 (dashed line), and CL0152-1357 and MS1054 (dotted line). There are no statistically significant differences between any of the samples, and also note that our sample size is small.

red inward color gradients, similar to field galaxies at low redshifts (de Jong 1996; Moth & Elston 2002), most of which are late-type. It should be stressed that this rough estimate of color gradient measures color relatively within a given galaxy. For example, if all cluster galaxies had positive values of CGE (blue inward) and all field galaxies had negative values (red inward), this would not necessarily mean that cluster galaxies have bluer centers than field galaxies, only that cluster galaxies have blue centers relative to the colors of their outer disks.

From Figure 9 it appears that more cluster galaxies have blue inward color gradients, but the difference between the overall field and cluster populations is not statistically significant. A K-S test indicates that the two distributions are not drawn from the same parent population at the 82% level, which we do not consider to be significant. The Wilcoxon rank-sum test, also referred to as the Mann-Whitney U-test, which is more sensitive to differences in the mean of distributions, finds a difference of approximately the same significance; the populations have a 85% probability of not having the same mean of distribution, which we also do not consider significant. If we choose our sample to include only those galaxies with rest-frame $U-B < 1.0$, effectively removing the red cluster sequence members, then the difference in color gradient is much more significant, as shown in the right panel of Figure 9. Here a K-S test shows a significant (97%) difference between the distributions of CGE; more of the blue cluster galaxies have blue inward color gradients. However, this cluster sample is still significantly redder than the field sample.

Any difference in color gradient should be due to a difference in the pattern of star formation. Relatively blue centers in the cluster galaxies could indicate enhanced nuclear star formation. The evidence for the existence of enhanced nuclear star formation in Virgo spirals (Koopmann & Kenney 2004), late-type galaxies in Abell clusters (Moss & Whittle 2000), indicates that this is a possible interpretation of our results.

We note that color gradient differences between cluster and field *early-type*, or spherodial, galaxies have also been found, but in an opposite sense. Some fraction ($\sim$ 30%) of field early-type galaxies have blue inward color gradients that indicate a later or more extended formation epoch, whereas cluster early-type have the red inward color gradients expected from metallicity gradients (Menanteau et al. 2001, 2004).

In summary, compared to the field late-type galaxies, we find that more cluster late-types have blue centers relative to the color of their outer disks. These relatively blue centers could indicate enhanced nuclear star formation rates, perhaps from gas driven in to the galaxy centers from tidal forces. They could also be the result of truncated gas disks like those seen in Virgo spirals (Koopmann & Kenney 2004).

4. DISCUSSION AND CONCLUSIONS

We find a difference in the rest-frame U and B asymmetry distributions of the spiral and irregular galaxies in the X-ray luminous (CL0152 and MS1054) and the X-ray faint (CL1604+4304 and CL1604+4321) clusters. The significance of these differences is marginal. However, a visual examination of the galaxies in these four clusters seems to confirm that at least the CL1604 system includes more peculiar systems (such as "comet-like" shapes) than CL0152 and MS1054.

An increase in the sample size of clusters is needed to confirm or refute this result, but if confirmed, it would provide evidence for an increased importance of interactions in low-mass clusters and the field relative to high-mass clusters at intermediate redshifts. Qualitatively, this may be plausible, as the relative velocities should be smaller in less massive clusters ($\sigma_v \propto M^{1/2}$). However, the magnitude of the difference in velocity dispersion between these clusters is small, and complicated by substructure. For example, the total velocity dispersion for CL0152 is $\sim$ 1600 km s^{-1} (Demarco et al. 2005), but can be decomposed into three subclumps with velocity dispersions ranging from $300 - 900$ km s^{-1} (Girardi et al. 2005). The velocity dispersion for MS1054 is $\sim 1100 - 1200$ km s^{-1} (Tran et al. 1999), while for CL1604+4304 and CL1604+4321 the velocity dispersions are $\sim$ 960 and $\sim$ 650 km s^{-1} (Gal & Lubin 2004), respectively. Since CL1604+4321 dominates the X-ray faint cluster sample, the difference in velocity dispersion between the two composite clusters (X-ray faint and X-ray luminous) is about a factor of 2.

Most significantly, the color distributions of the cluster and field spiral/irregular galaxies differ, with the cluster sample being significantly redder. At the same time, we tentatively find that more cluster galaxies have blue inward color gradients, possibly indicating enhanced central star formation relative to the outer disk.

To interpret these results, it is useful to consider observations of cluster spirals in the local universe, where we have the best chance of studying environmental processes in detail. Using Hα imaging of Virgo cluster spirals, Koopmann & Kenney (2004) showed that the reduction in overall SFR for spiral galaxies in local clusters is due to a truncation of the gas disk. Star formation rates in the centers of spiral galaxies in the cluster and field are similar, but the lack of gas at outer radii in cluster spirals means that the overall SFRs are suppressed. The physical mechanism identified as responsible for this gas disk truncation is ram pressure stripping, which could be aided by tidal loosening of the outer gas (Koopmann & Kenney 2004). Also, color gradients in low-redshift cluster and field galaxies with overall blue colors differ, with field galaxies having red inward color gradients and cluster galaxies having blue inward color gradients (McIntosh et al. 2004). This may be circumstantial evidence that these blue cluster galaxies have relatively enhanced nuclear SFRs similar to Virgo spirals.

There is other evidence that gas is driven to the centers of cluster spirals and causes circumnuclear starbursts. The study of low-redshift Abell clusters by Moss & Whittle (2000) found that enhanced nuclear star formation, as traced by Hα emission, was correlated with either a bar, or disturbed galaxy morphology, which they concluded was evidence for ongoing tidal interactions. However, they found an increase in galaxies classified as peculiar with increasing local galaxy density, something which is not consistent with the overall morphology-density relation.

Tran et al. (2005) studied the MS 2053 cluster system at $z = 0.587$ and concluded that the spiral/merger galaxy population in MS 2053-B is indistinguishable from the field in terms of colors, luminosities, sizes, and [OII] λ3727 EW. They conclude that this is an infalling field population. However, the colors of the spiral/merger population in the more massive MS 2053-A are different than those in MS 2053-B and the field. They are redder on average, similar to what we find here.

We interpret these findings as evidence that although some blue cluster galaxies may be identified as infalling field galaxies, *as an ensemble, the late-type cluster members at intermediate redshifts are not a pristine infalling field population.* There are significant differences between cluster and field late-type galaxies even at these redshifts. Most of the cluster late-type galaxies are more than two standard deviations away from the observed red cluster sequence, meaning that these are Butcher-Oemler galaxies. Even given such blue colors, they are still redder than field galaxies.

This may be further evidence for the separate evolution of color and morphology (e.g. Goto et al. 2003, McIntosh et al. 2004) in high density environments. The evolution in color occurs faster than the evolution in morphology. This is puzzling, because the only mechanisms which would affect a galaxy's color on a longer timescale than its morphology will also alter the *gas content.* The only mechanisms which could alter the gas content and not the morphology (at least directly) are ram-pressure stripping and starvation. But these are not expected to be important because the morphology-density and color-density relations are in place in low density regions where ICM or intra-group medium pressure is negligible. If the ICM is unimportant, but color differences occur in lower density regions than morphology differences, does this mean that nature is more important than nurture?

Our comparison of cluster and field late-type galaxies at intermediate redshift shows that while the cluster galaxies are similar in most physical parameters, they are signficantly redder. The color transformation is perhaps occuring at these or higher redshifts in lower density groups, with clusters accreting such groups with "pre-processed" galaxies along filaments (e.g. Kodama et al. 2001).

Our main conclusions are as follows.

- The late-type cluster population is redder than the late-type field population. This is our most significant result. The mean rest-frame $U - B$ color difference is 0.34 magnitudes between the combined cluster (X-ray luminous and X-ray faint) and field

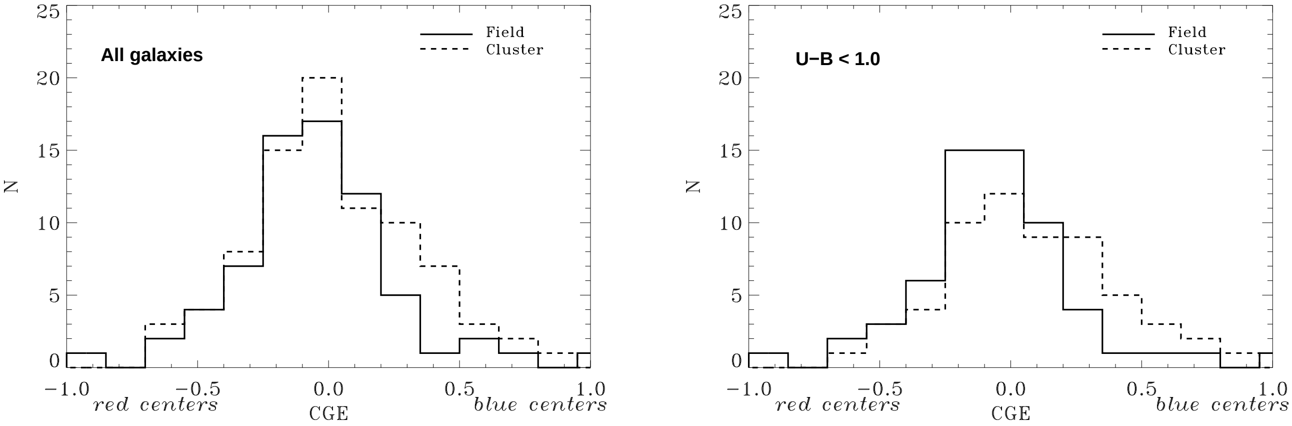

FIG. 9.— Comparison of the field (solid line) and cluster (dashed line) color gradients. In the left panel, we compare the complete samples. In the right panel, we only include those galaxies bluer than $U - B = 1$, effectively removing the red cluster sequence galaxies. There is no statistically significant difference between the complete cluster and field samples, and a marginally significant difference in the blue samples (97%). The blue cluster galaxies tend to have blue inward color gradients.

samples. Although individual galaxies may be infalling from the field, as an ensemble, they cannot be identified as a pristine infalling population.

- At both rest-frame U and B, we find a marginally significant difference (98%, 99%) in the asymmetry distributions of the late-type galaxies in the X-ray luminous clusters and the field. Late-type galaxies in X-ray luminous clusters have lower asymmetries than those in the field. However, this difference can be completely attributed to the difference in rest-frame color. Considering only those galaxies bluer than $U - B = 1$, which removes the red cluster sequence galaxies, the asymmetry distributions are indistinguishable.
- At both rest-frame U and B, we find a marginally significant difference (99%, 92%) in the asymmetry distributions of the late-type galaxies in the X-ray luminous clusters and the X-ray faint clusters. Galaxies in the X-ray faint clusters have larger asymmetry values than those in X-ray luminous clusters. This asymmetry difference persists when the red cluster sequence galaxies are removed and only the blue galaxies are considered (99%). If confirmed when the cluster and field sample sizes are increased, this could point to a greater importance of interactions in lower density regions at these redshifts.
- We find no significant differences between any of the samples in concentration or clumpiness at rest-frame U and B.
- Physical sizes of field and cluster late-type galaxies are similar. We find no significant difference in galaxy size as measured by half-light radii and disk scale lengths.
- Considering only the blue ($U - B < 1$) cluster and field galaxies, we find a marginally significant difference in the distributions of color gradients for the cluster and field late-type populations. We find that more blue cluster galaxies have bluer inward gradients, possibly indicating enhanced nuclear star formation as is seen in low redshift clusters (Koopmann & Kenney 2004; McIntosh et al. 2004).

While similar in structure, physical size, and luminosity, the infalling late-type galaxies in the outer cluster regions are redder and appear to have had a different star formation history than their late-type field counterparts. This suggests that their assembly has already been influenced by the somewhat denser environment in which they evolved.

We thank the referee for a careful reading and suggestions which improved the clarity of the manuscript. We also thank T. Puzia for reading and commenting on an early version of this paper. ACS was developed under NASA contract NAS 5-32865, and this research has been supported by NASA grant NAG5-7697 and by an equipment grant from Sun Microsystems, Inc. The Space Telescope Science Institute is operated by AURA Inc., under NASA contract NAS5-26555. We are grateful to K. Anderson, J. McCann, S. Busching, A. Framarini, S. Barkhouser, and T. Allen for their invaluable contributions to the ACS project at JHU. We thank W. J. McCann for the use of the FITSCUT routine for our color images.

REFERENCES

Abraham, R. G., Valdes, F., Yee, H. K. C., & van den Bergh, S. 1994, ApJ, 432, 75
Balogh, M. L., Morris, S. L., Yee, H. K. C., Carlberg, R. G., & Ellingson, E. 1997, ApJ, 488, L75
Balogh, M. L., Schade, D., Morris, S. L., Yee, H. K. C., Carlberg, R. G., & Ellingson, E. 1998, ApJ, 504, L75
Balogh, M., et al. 2004, MNRAS, 348, 1355
Bekki, K., Couch, W. J., & Shioya, Y. 2002, ApJ, 577, 651

TABLE 2
CL1604+4304

ACS ID	C 606	C 814	A 606	A 814	S 606	S 814	r_e 606	r_e 814	$v_{606} - i_{814}$	i_{814}
2933	0.251	0.239	0.210	0.156	0.119	0.099	—	—	0.73±0.05	24.29 ±0.04
2531	0.466	0.474	0.209	0.151	0.032	0.012	***	5.9	1.25±0.02	22.37 ±0.01
2930	0.219	0.256	0.309	0.309	0.128	0.049	—	—	1.59±0.02	21.84 ±0.01
1495	0.326	0.337	0.151	0.149	0.091	0.046	16.9	18.3	1.63±0.01	20.85 ±0.00
1627	0.401	0.349	0.340	0.304	0.087	0.073	—	—	0.54±0.02	22.53 ±0.02
1448	0.283	0.260	0.268	0.197	0.051	0.041	9.2	11.4	0.64±0.01	22.24 ±0.01
2121	0.496	0.438	0.154	0.140	0.030	0.021	—	—	0.86±0.02	22.68 ±0.01
1135	0.315	0.336	0.385	0.379	0.028	0.011	16.5	17.0	1.33±0.01	21.99 ±0.01
2701	0.667	0.543	0.209	0.183	0.003	0.002	—	—	0.94±0.02	22.99 ±0.01

Note. — Asterisks indicate that 2D profile fitting with GALFIT was attempted, but did not converge. Effective radii are quoted in pixels (1 pixel=0.05$''$). Redshifts are given in the second column for field galaxies.

Benítez, N., et al. 2004, ApJS, 150, 1
Bershady, M. A., Jangren, A., & Conselice, C. J. 2000, AJ, 119, 2645
Bertin, E., & Arnouts, S. 1996, A&AS, 117, 393
Blakeslee, J. P., Anderson, K. R., Meurer, G. R., Benítez, N., & Magee, D. 2003, Astronomical Society of the Pacific Conference Series, 295, 257
Blakeslee, J. P., et al. 2003, ApJ, 596, L143
Butcher, H., & Oemler, A. 1984, ApJ, 285, 426
Conselice, C. J. 2003, ApJS, 147, 1
Couch, W. J., Balogh, M. L., Bower, R. G., Smail, I., Glazebrook, K., & Taylor, M. 2001, ApJ, 549, 820
de Jong, R. S. 1996, A&A, 313, 377
de Vaucouleurs, G., de Vaucouleurs, A., Corwin, H. G., Buta, R. J., Paturel, G., & Fouque, P. 1991, Volume 1-3, XII, 2069 pp. 7 figs.. Springer-Verlag Berlin Heidelberg New York,
Demarco, R., et al. 2005, A&A, 432, 381
Dressler, A. 1980, ApJ, 236, 351
Dressler, A., et al. 1997, ApJ, 490, 577
Ellingson, E., Lin, H., Yee, H. K. C., & Carlberg, R. G. 2001, ApJ, 547, 609
Finn, R. A., Zaritsky, D., & McCarthy, D. W. 2004, ApJ, 604, 141
Finn, R. A., et al. 2005, ArXiv Astrophysics e-prints, arXiv:astro-ph/0504578
Ford, H. C., et al. 2003, Proc. SPIE, 4854, 81
Fujita, Y. & Nagashima, M. 1999, ApJ, 516, 619
Gal, R. R., & Lubin, L. M. 2004, ApJ, 607, L1
Girardi, M., Demarco, R., Rosati, P., Borgani, S., A&A, submitted
Gómez, P. L., et al. 2003, ApJ, 584, 210
Goto, T., et al. 2003, PASJ, 55, 757
Goto, T., Yagi, M., Tanaka, M., & Okamura, S. 2004, MNRAS, 348, 515
Goto, T. et al., ApJ, 621, 188
Gunn, J. E., & Gott, J. R. I. 1972, ApJ, 176, 1
Gutiérrez, C. M., Trujillo, I., Aguerri, J. A. L., Graham, A. W., & Caon, N. 2004, ApJ, 602, 664
Hashimoto, Y., Oemler, A. J., Lin, H., & Tucker, D. L. 1998, ApJ, 499, 589
Holden, B. P., et al. 2005, ApJ, 620, L83
Holden, B. et al., ApJ, 626, 809
Homeier, N. L., et al. 2005, ApJ, 621, 651
Kauffmann, G., White, S. D. M., Heckman, T. M., Ménard, B., Brinchmann, J., Charlot, S., Tremonti, C., & Brinkmann, J. 2004, MNRAS, 353, 713
Kinney, A. L., Calzetti, D., Bohlin, R. C., et al. 1996, ApJ, 467, 38
Kodama, T., Smail, I., Nakata, F., Okamura, S., & Bower, R. G. 2001, ApJ, 562, L9
Kodama, T., Balogh, M. L., Smail, I., Bower, R. G., & Nakata, F. 2004, MNRAS, 354, 1103
Koopmann, R. A., & Kenney, J. D. P. 2004, ApJ, 613, 866
Larson, R. B., Tinsley, B. M., & Caldwell, C. N. 1980, ApJ, 237, 692
Lewis, I., et al. 2002, MNRAS, 334, 673
Lubin, L. M., Postman, M., Oke, J. B., Ratnatunga, K. U., Gunn, J. E., Hoessel, J. G., & Schneider, D. P. 1998, AJ, 116, 584
Martínez, H. J., Zandivarez, A., Domínguez, M., Merchán, M. E., & Lambas, D. G. 2002, MNRAS, 333, L31
McIntosh, D. H., Rix, H., & Caldwell, N. 2004, ApJ, 610, 161
Menanteau, F., Abraham, R. G., & Ellis, R. S. 2001, MNRAS, 322, 1
Menanteau, F., et al. 2004, ApJ, 612, 202
Menanteau, F., et al., in preparation
Moore, B., Lake, G., & Katz, N. 1998, ApJ, 495, 139
Moss, C., & Whittle, M. 2000, MNRAS, 317, 667
Moth, P., & Elston, R. J. 2002, AJ, 124, 1886
Nakata, F., Bower, R. G., Balogh, M. L., & Wilman, D. J. 2005, MNRAS, 59
Peng, C. Y., Ho, L. C., Impey, C. D., & Rix, H. 2002, AJ, 124, 266
Postman, M., & Geller, M. J. 1984, ApJ, 281, 95
Postman, M., Lubin, L. M., & Oke, J. B. 1998, AJ, 116, 560
Postman, M., Lubin, L. M., & Oke, J. B. 2001, AJ, 122, 1125
Postman, M., et al. 2005, ApJ, 623, 721
Quilis, V., Moore, B., & Bower, R. 2000, Science, 288, 1617
Roediger, E., & Hensler, G. 2005, A&A, 433, 875
Rose, J. A., Gaba, A. E., Caldwell, N., & Chaboyer, B. 2001, AJ, 121, 793
Schulz, S., & Struck, C. 2001, MNRAS, 328, 185
Smith, G. P., Treu, T., Ellis, R. S., Moran, S. M., & Dressler, A. 2005, ApJ, 620, 78
Tanaka, M., Goto, T., Okamura, S., Shimasaku, K., & Brinkmann, J. 2004, AJ, 128, 2677
Tran, K. H., Kelson, D. D., van Dokkum, P., Franx, M., Illingworth, G. D., & Magee, D. 1999, ApJ, 522, 39
Tran, K. H., van Dokkum, P., Illingworth, G. D., Kelson, D., Gonzalez, A., & Franx, M. 2005, ApJ, 619, 134
Wake, D. A., Collins, C. A., Nichol, R. C., Jones, L. R., Burke, D. J. 2005, ApJ, 627, 186
Whitmore, B. C., & Gilmore, D. M. 1991, ApJ, 367, 64

TABLE 3
CL1604+4304 FIELD SAMPLE

ACS ID	redshift	C 606	C 814	A 606	A 814	S 606	S 814	r_e 606	r_e 814	$v_{606} - i_{814}$	i_{814}
621	0.548	0.432	0.410	0.129	0.123	0.017	0.014	9.3	8.1	0.51±0.01	22.97 ±0.01
2166	0.609	0.361	0.364	0.196	0.149	0.048	0.040	—	—	0.62±0.01	22.26 ±0.01
681	0.742	0.247	0.278	0.152	0.104	0.056	0.037	12.5	11.8	0.90±0.02	22.56 ±0.01
2230	0.830	0.186	0.230	0.305	0.227	0.070	0.046	—	—	0.81±0.01	21.83 ±0.01
1984	0.833	0.330	0.297	0.149	0.115	0.065	0.034	8.0	7.1	1.39±0.02	21.95 ±0.01
1656	0.937	0.309	0.315	0.082	0.074	0.017	0.018	6.6	6.9	0.32±0.01	22.42 ±0.01
1389	0.973	0.219	0.237	0.122	0.098	0.070	0.052	9.0	12.4	0.80±0.02	22.53 ±0.01
2645	0.974	0.292	0.338	0.129	0.091	0.033	0.022	7.4	7.7	0.83±0.01	22.47 ±0.01
2539	0.985	0.289	0.364	0.156	0.098	0.082	0.033	—	—	1.42±0.02	21.74 ±0.01
1068	1.068	0.326	0.286	0.084	0.103	0.088	0.037	—	—	1.61±0.02	22.23 ±0.01
1374	1.085	0.613	0.538	0.176	0.244	0.004	0.005	4.4	7.2	0.24±0.01	22.78 ±0.01
802	1.096	0.237	0.235	0.232	0.139	0.061	0.050	9.3	10.2	0.61±0.02	22.91 ±0.01

TABLE 4
CL1604+4321

ACS ID	C 606	C 814	A 606	A 814	S 606	S 814	r_e 606	r_e 814	$v_{606} - i_{814}$	i_{814}
1547	0.332	0.258	0.303	0.322	0.065	0.058	—	—	0.63±0.02	23.45 ±0.02
990	0.175	0.180	0.224	0.218	0.117	0.071	—	—	1.13±0.02	22.69 ±0.02
1849	0.165	0.163	0.294	0.226	0.120	0.096	5.8	13.3	0.72±0.03	23.69 ±0.03
880	0.338	0.347	0.104	0.101	0.096	0.035	2.2	13.0	1.84±0.02	21.95 ±0.01
883	0.267	0.309	0.231	0.195	0.114	0.061	2.6	8.0	1.37±0.02	22.21 ±0.01
1459	0.399	0.423	0.213	0.141	0.067	0.028	7.2	14.4	1.12±0.01	21.28 ±0.01
1640	0.210	0.293	0.174	0.140	0.136	0.060	1.6	***	1.50±0.01	21.47 ±0.01
3443	0.272	0.287	0.132	0.093	0.033	0.021	4.3	4.7	1.07±0.02	23.05 ±0.01
2238	0.353	0.363	0.122	0.111	0.056	0.022	7.6	9.6	1.52±0.02	22.16 ±0.01
1892	0.491	0.502	0.098	0.043	0.030	0.007	***	6.0	1.75±0.02	21.87 ±0.01
1034	0.229	0.247	0.152	0.135	0.068	0.048	7.0	***	0.85±0.02	23.27 ±0.02
2195	0.305	0.275	0.226	0.192	0.028	0.025	5.6	***	0.70±0.02	22.97 ±0.01
2272	0.300	0.239	0.264	0.194	0.131	0.072	***	16.3	1.31±0.02	22.09 ±0.01
1341	0.244	0.196	0.091	0.079	0.036	0.028	6.5	5.4	0.98±0.02	23.35 ±0.02
2865	0.239	0.277	0.205	0.151	0.089	0.061	10.5	8.4	0.82±0.02	22.81 ±0.02
1930	0.200	0.216	0.159	0.112	0.053	0.037	9.3	8.5	1.01±0.01	21.96 ±0.01
1142	0.440	0.355	0.107	0.128	0.017	0.012	—	—	0.94±0.02	23.30 ±0.01
2470	0.235	0.307	0.068	0.064	0.119	0.042	***	10.2	1.50±0.02	22.24 ±0.01
2283	0.257	0.249	0.170	0.124	0.056	0.037	***	8.1	0.98±0.02	22.55 ±0.01
783	0.159	0.129	0.256	0.261	0.149	0.090	—	—	1.07±0.04	23.54 ±0.03
694	0.422	0.380	0.262	0.273	0.025	0.021	—	—	0.62±0.01	22.75 ±0.01
1160	0.296	0.293	0.315	0.262	0.047	0.036	—	—	0.89±0.01	22.08 ±0.01
2605	0.264	0.235	0.223	0.140	0.164	0.075	—	—	1.44±0.02	22.37 ±0.01

TABLE 5
CL1604+4321 FIELD SAMPLE

ACS ID	redshift	C 606	C 814	A 606	A 814	S 606	S 814	r_e 606	r_e 814	$v_{606} - i_{814}$	i_{814}
2338	0.618	0.407	0.414	0.121	0.093	0.015	0.011	8.9	8.1	0.77±0.01	21.56 ±0.01
1071	0.618	0.459	0.417	0.211	0.145	0.009	0.010	5.9	4.7	0.44±0.02	23.38 ±0.02
1596	0.694	0.548	0.467	0.295	0.279	0.076	0.054	—	—	1.00±0.01	21.34 ±0.01
1655	0.695	0.288	0.309	0.281	0.235	0.051	0.037	8.3	7.4	0.84±0.01	22.40 ±0.01
2143	0.696	0.293	0.267	0.267	0.214	0.056	0.047	25.8	25.1	0.71±0.01	21.59 ±0.01
2140	0.715	0.248	0.253	0.162	0.117	0.056	0.032	***	12.4	1.32±0.02	22.29 ±0.01
2220	0.726	0.350	0.335	0.255	0.206	0.032	0.027	6.4	4.6	0.64±0.01	22.46 ±0.01
1572	0.726	0.219	0.266	0.072	0.048	0.034	0.025	5.6	5.2	0.64±0.02	23.32 ±0.01
1878	1.099	0.374	0.399	0.141	0.137	0.104	0.036	10.1	13.0	1.74±0.02	22.20 ±0.01
1017	1.128	0.327	0.233	0.372	0.298	0.182	0.095	10.6	11.3	1.48±0.02	22.02 ±0.01
966	1.174	0.239	0.231	0.222	0.181	0.040	0.036	8.8	10.1	0.85±0.32	27.48 ±0.21
1438	1.182	0.252	0.175	0.267	0.301	0.150	0.104	—	—	0.91±0.03	23.44 ±0.03

TABLE 6
MS1054

ACS ID	C 606	C 775	A 606	A 775	S 606	S 775	r_e 606	r_e 775	$v_{606} - i_{775}$	$i_{775} - z_{850}$	i_{775}
392	0.293	0.329	0.182	0.150	0.081	0.034	8.6	8.8	0.83±0.02	0.17±0.02	22.33±0.01
456	0.521	0.411	0.107	0.087	0.065	0.029	1.6	***	0.96±0.03	0.34±0.03	23.07±0.02
835	0.196	0.220	0.289	0.256	0.144	0.090	—	18.1	0.67±0.03	0.10±0.03	22.80±0.03
947	0.186	0.194	0.098	0.068	0.075	0.035	6.2	***	1.51±0.02	0.54±0.01	21.66±0.01
921	0.351	0.364	0.108	0.124	0.103	0.032	6.7	6.9	0.93±0.04	0.20±0.03	23.44±0.02
959	0.388	0.335	0.194	0.175	0.160	0.056	1.3	1.4	1.21±0.03	0.43±0.02	22.65±0.02
1484	0.271	0.271	0.187	0.171	0.181	0.094	***	2.4	0.67±0.05	0.13±0.05	23.71±0.04
1948	0.242	0.199	0.220	0.179	0.135	0.079	***	54.0	1.08±0.01	0.27±0.01	20.53±0.01
2013	0.463	0.411	0.073	0.100	0.059	0.020	6.4	7.6	1.14±0.02	0.45±0.01	22.62±0.01
2210	0.432	0.465	0.093	0.110	0.021	0.006	4.7	6.5	1.39±0.02	0.48±0.01	22.43±0.01
2586	0.263	0.252	0.109	0.128	0.058	0.027	5.2	***	0.96±0.03	0.15±0.03	23.00±0.02
2813	0.297	0.341	0.076	0.068	0.136	0.035	1.7	9.2	1.47±0.02	0.61±0.01	21.47±0.01
2879	0.261	0.241	0.135	0.117	0.058	0.041	6.7	***	0.51±0.04	0.15±0.04	23.87±0.03
3070	0.229	0.250	0.167	0.140	0.115	0.062	5.4	***	1.12±0.03	0.39±0.02	22.57±0.01
2976	0.326	0.317	0.084	0.079	0.066	0.030	3.0	***	0.93±0.02	0.45±0.01	21.51±0.01
3075	0.355	0.382	0.077	0.096	0.039	0.016	9.4	13.3	1.44±0.01	0.43±0.00	20.82±0.00
3299	0.294	0.289	0.094	0.094	0.180	0.053	—	—	1.45±0.06	0.57±0.03	23.30±0.03
3322	0.216	0.266	0.100	0.117	0.040	0.019	4.3	4.7	0.67±0.03	0.09±0.03	23.24±0.02
3340	0.242	0.247	0.281	0.266	0.086	0.046	—	—	0.80±0.02	0.20±0.02	22.49±0.02
3403	0.346	0.359	0.193	0.201	0.040	0.021	4.5	4.9	0.68±0.02	0.24±0.02	22.57±0.01
3438	0.167	0.197	0.234	0.189	0.124	0.053	6.9	7.4	1.03±0.03	0.35±0.02	22.62±0.02
3727	0.203	0.207	0.137	0.154	0.112	0.083	—	—	0.34±0.03	0.06±0.04	22.89±0.03
3802	0.279	0.251	0.152	0.123	0.059	0.033	8.4	8.7	0.79±0.02	0.29±0.01	22.28±0.01
4101	0.230	0.240	0.263	0.221	0.175	0.074	5.8	6.7	1.02±0.03	0.37±0.01	22.21±0.01
4234	0.310	0.251	0.546	0.638	0.042	0.038	—	—	0.45±0.01	0.15±0.01	21.07±0.00
4777	0.279	0.263	0.152	0.177	0.061	0.034	—	—	1.17±0.01	0.32±0.01	21.94±0.01
5040	0.255	0.287	0.158	0.144	0.050	0.031	5.2	***	0.76±0.01	0.25±0.01	21.51±0.01
5152	0.190	0.202	0.082	0.127	0.118	0.055	—	—	1.15±0.03	0.31±0.02	23.36±0.02
5967	0.181	0.193	0.212	0.207	0.174	0.083	—	3.3	0.77±0.03	0.21±0.02	22.37±0.02
6567	0.224	0.225	0.166	0.159	0.088	0.045	6.1	9.0	0.78±0.02	0.27±0.02	22.60±0.02
6872	0.207	0.231	0.136	0.128	0.112	0.050	4.0	6.1	1.00±0.03	0.34±0.02	22.43±0.02
9133	0.381	0.380	0.120	0.111	0.108	0.034	***	6.0	1.34±0.03	0.46±0.01	22.04±0.01

TABLE 7
MS1054 field sample

ACS ID	redshift	C 606	C 775	A 606	A 775	S 606	S 775	r_e 606	r_e 775	$v_{606} - i_{775}$	$i_{775} - z_{850}$	i_{775}
1191	0.552	0.317	0.339	0.139	0.200	0.108	0.043	8.2	8.4	1.25±0.04	0.41±0.02	22.84±0.02
1542	0.553	0.252	0.303	0.149	0.159	0.091	0.035	3.7	16.2	0.560 ± 0.01	0.12 ± 0.01	21.60 ± 0.01
556	0.559	0.279	0.280	0.176	0.205	0.056	0.038	—	—	0.75±0.01	0.21±0.01	21.48±0.01
1401	0.561	0.180	0.222	0.183	0.161	0.106	0.067	***	2.0	0.56±0.02	0.08±0.02	21.66±0.01
2478	0.573	0.361	0.310	0.077	0.076	0.046	0.027	—	—	0.73±0.02	0.20±0.02	22.97±0.02
531	0.580	0.230	0.257	0.344	0.316	0.109	0.087	20.0	19.9	0.48±0.02	-0.03±0.02	22.31±0.01
5659	0.600	0.260	0.273	0.302	0.288	0.087	0.061	—	—	0.56±0.02	0.02±0.02	21.99±0.01
3573	0.617	0.223	0.223	0.109	0.081	0.067	0.053	7.9	9.0	0.21±0.02	0.12±0.03	23.12±0.02
3865	0.618	0.256	0.253	0.088	0.076	0.059	0.041	2.6	7.8	0.36±0.02	0.10±0.02	22.23±0.01
9272	0.666	0.470	0.447	0.106	0.087	0.007	0.004	3.8	3.0	0.67±0.01	0.15±0.01	22.36±0.01
3523	0.702	0.217	0.222	0.339	0.341	0.139	0.086	—	—	0.62±0.02	0.11±0.02	22.20±0.02
9214	0.702	0.234	0.242	0.183	0.176	0.079	0.046	9.4	1.8	0.88±0.01	0.26±0.01	21.19±0.01
8165	0.702	0.171	0.202	0.190	0.178	0.075	0.039	—	—	0.66±0.04	0.13±0.04	23.80±0.03
5464	0.715	0.323	0.370	0.124	0.130	0.049	0.025	5.6	4.0	1.07±0.01	0.45±0.01	22.20±0.01
6284	0.756	0.181	0.184	0.190	0.184	0.126	0.066	4.4	15.6	0.80±0.02	0.24±0.02	22.04±0.01
4324	0.759	0.462	0.464	0.209	0.183	0.021	0.014	3.4	3.5	1.30±0.02	0.41±0.01	22.21±0.01
1203	0.761	0.314	0.282	0.257	0.213	0.071	0.050	4.4	4.8	0.53±0.01	0.14±0.01	21.55±0.01
7248	0.761	0.234	0.320	0.163	0.137	0.147	0.057	4.5	1.9	1.13±0.01	0.43±0.01	21.20±0.01
7538	0.762	0.579	0.499	0.113	0.103	0.013	0.008	1.6	1.1	0.81±0.01	0.30±0.01	22.57±0.01
6320	0.762	0.168	0.187	0.401	0.390	0.113	0.067	4.1	34.9	0.94±0.02	0.29±0.01	21.59±0.01
3970	0.778	0.228	0.234	0.230	0.169	0.058	0.036	4.1	***	0.53±0.03	0.13±0.03	23.51±0.02
7987	0.870	0.199	0.212	0.266	0.292	0.069	0.050	7.7	3.1	0.47±0.01	0.18±0.01	21.78±0.01
4887	0.873	0.404	0.381	0.203	0.181	0.031	0.021	4.3	4.1	0.84±0.01	0.25±0.01	22.25±0.01
1560	0.896	0.155	0.198	0.269	0.264	0.246	0.116	—	—	0.95±0.02	0.34±0.01	21.31±0.01
305	0.897	0.252	0.265	0.149	0.131	0.078	0.039	5.7	7.0	0.75±0.03	0.22±0.02	22.76±0.02
7225	0.897	0.205	0.241	0.223	0.177	0.103	0.056	4.7	4.3	0.66±0.03	0.21±0.03	23.25±0.02
2643	0.897	0.133	0.147	0.260	0.244	0.189	0.105	—	—	0.71±0.03	0.33±0.03	22.71±0.03
6423	0.971	0.163	0.183	0.135	0.141	0.069	0.044	4.2	***	0.58±0.03	0.24±0.03	23.49±0.03
1668	0.978	0.131	0.176	0.143	0.189	0.214	0.101	—	—	0.78±0.06	0.35±0.05	23.79±0.05
1021	0.990	0.163	0.160	0.121	0.143	0.127	0.087	6.0	4.4	0.31±0.06	0.59±0.06	24.35±0.07
2991	1.060	0.223	0.157	0.287	0.310	0.373	0.130	—	—	1.19±0.09	0.76±0.04	23.80±0.05
5649	1.073	0.212	0.257	0.187	0.134	0.041	0.025	—	—	0.56±0.03	0.37±0.03	23.67±0.03
3881	1.075	0.501	0.476	0.272	0.297	0.029	0.025	—	—	0.51±0.01	0.24±0.01	21.32±0.00
3046	1.076	0.142	0.190	0.189	0.198	0.078	0.049	—	—	1.08 ± 0.05	0.71 ± 0.03	23.44 ± 0.04
1289	1.140	0.241	0.258	0.166	0.197	0.055	0.040	5.3	10.1	0.33±0.03	0.41±0.03	23.38±0.03

TABLE 8
CL0152-1357

ACS ID	C 625	C 775	A 625	A 775	S 625	S 775	r_e 625	r_e 775	$r_{625} - i_{775}$	$i_{775} - z_{850}$	i_{775}
10063	0.402	0.392	0.134	0.109	0.070	0.039	—	—	0.95±0.02	0.44±0.02	22.65±0.01
11019	0.430	0.496	0.097	0.075	0.022	0.007	—	—	1.09±0.02	0.65±0.01	22.68±0.01
11613	0.271	0.287	0.118	0.107	0.062	0.030	—	—	1.04±0.03	0.48±0.02	23.06±0.01
1146	0.217	0.239	0.127	0.122	0.038	0.038	7.8	12.2	0.74±0.02	0.32±0.02	22.58±0.02
1564	0.392	0.361	0.183	0.189	0.056	0.037	7.6	4.6	0.78±0.02	0.33±0.02	22.66±0.02
1575	0.314	0.354	0.125	0.084	0.045	0.036	4.9	***	1.06±0.04	0.70±0.02	22.88±0.02
1652	0.247	0.263	0.157	0.119	0.063	0.044	8.7	8.6	0.80±0.01	0.28±0.01	21.63±0.01
1737	0.207	0.215	0.131	0.114	0.077	0.042	3.0	2.1	1.03±0.02	0.42±0.02	22.79±0.01
2016	0.450	0.412	0.420	0.404	0.052	0.050	—	—	0.26±0.01	0.12±0.02	22.28±0.01
2027	0.240	0.302	0.317	0.246	0.094	0.055	9.6	11.2	0.88±0.02	0.42±0.01	22.13±0.01
2235	0.453	0.457	0.118	0.106	0.056	0.023	14.1	4.8	1.24±0.02	0.60±0.01	21.70±0.01
3329	0.645	0.539	0.352	0.300	0.066	0.049	—	—	0.80±0.01	0.62±0.00	20.62±0.00
3390	0.317	0.349	0.121	0.103	0.126	0.052	1.3	2.5	1.20±0.02	0.70±0.01	21.07±0.01
3927	0.265	0.292	0.271	0.260	0.087	0.061	10.8	11.8	0.84±0.01	0.33±0.01	21.57±0.01
5410	0.478	0.439	0.138	0.138	0.048	0.024	6.1	9.3	1.02±0.01	0.48±0.01	21.59±0.01
5481	0.329	0.387	0.212	0.174	0.057	0.031	3.5	10.5	1.04±0.01	0.63±0.01	22.02±0.01
7017	0.393	0.420	0.092	0.077	0.049	0.027	2.0	7.5	1.14±0.01	0.57±0.01	21.25±0.01
717	0.317	0.327	0.093	0.098	0.101	0.043	7.3	***	1.26±0.03	0.60±0.02	22.43±0.02
8671	0.207	0.234	0.224	0.187	0.078	0.057	11.2	10.1	0.72±0.01	0.30±0.01	21.41±0.01
8708	0.162	0.180	0.132	0.082	0.070	0.043	6.9	5.7	0.57±0.03	0.26±0.03	23.44±0.02
9563	0.498	0.546	0.152	0.087	0.029	0.013	—	—	1.23±0.02	0.57±0.01	22.08±0.01

TABLE 9
CL0152 FIELD SAMPLE

ACS ID	redshift	C 606	C 775	A 606	A 775	S 606	S 775	r_e 625	r_e 775	$r_{625} - i_{775}$	$i_{775} - z_{850}$	i_{775}
668	0.556	0.399	0.388	0.171	0.168	0.027	0.021	—	—	0.46±0.01	0.22±0.01	21.35±0.01
1051	0.670	0.406	0.449	0.222	0.211	0.079	0.054	5.0	5.2	0.75±0.01	0.35±0.01	21.24±0.01
2199	0.675	0.242	0.229	0.222	0.246	0.072	0.084	12.3	12.2	-0.01±0.03	-0.03±0.05	24.29±0.04
978	0.720	0.280	0.316	0.118	0.120	0.033	0.025	10.1	8.8	0.58±0.01	0.19±0.01	21.91±0.01
2399	0.739	0.474	0.469	0.104	0.088	0.029	0.025	—	—	0.37±0.00	0.28±0.01	21.11±0.00
2456	0.746	0.271	0.305	0.214	0.192	0.038	0.031	11.1	11.3	0.42±0.02	0.23±0.03	23.70±0.02
5222	0.788	0.494	0.541	0.097	0.092	0.029	0.009	2.3	2.5	1.16±0.01	0.58±0.01	21.64±0.01
8851	0.959	0.160	0.154	0.274	0.266	0.148	0.093	—	—	0.84±0.04	0.47±0.03	23.12±0.03
5804	0.960	0.278	0.298	0.201	0.163	0.066	0.043	12.6	9.7	0.79±0.01	0.43±0.01	21.70±0.01
805	0.993	0.534	0.456	0.206	0.219	0.030	0.024	1.7	***	0.48±0.01	0.41±0.01	21.72±0.01
8441	1.048	0.414	0.391	0.179	0.152	0.037	0.032	14.9	14.7	0.47±0.02	0.40±0.02	22.71±0.01
6851	1.101	0.257	0.234	0.287	0.246	0.077	0.066	—	—	0.42±0.01	0.42±0.01	22.25±0.01
6879	1.120	0.149	0.167	0.284	0.280	0.119	0.095	24.0	23.6	0.55±0.01	0.62±0.01	21.94±0.01